TISSUE ENGINEERING: Part A
Volume 18, Numbers 5 and 6, 2012

DOI: 10.1089/ten.tea.2011.0279

A Hydrogel-Mineral Composite Scaffold for Osteochondral Interface Tissue Engineering

Nora T. Khanarian, M.S.,[1] Jie Jiang, Ph.D.,[1] Leo Q. Wan, Ph.D.,[2] Van C. Mow, Ph.D.,[2] and Helen H. Lu, Ph.D.[1]

Osteoarthritis is the leading cause of physical disability among Americans, and tissue engineered cartilage grafts have emerged as a promising treatment option for this debilitating condition. Currently, the formation of a stable interface between the cartilage graft and subchondral bone remains a significant challenge. This study evaluates the potential of a hybrid scaffold of hydroxyapatite (HA) and alginate hydrogel for the regeneration of the osteochondral interface. Specifically, the effects of HA on the response of chondrocytes were determined, focusing on changes in matrix production and mineralization, as well as scaffold mechanical properties over time. Additionally, the optimal chondrocyte population for interface tissue engineering was evaluated. It was observed that the HA phase of the composite scaffold promoted the formation of a proteoglycan- and type II collagen–rich matrix when seeded with deep zone chondrocytes. More importantly, the elevated biosynthesis translated into significant increases in both compressive and shear moduli relative to the mineral-free control. Presence of HA also promoted chondrocyte hypertrophy and type X collagen deposition. These results demonstrate that the hydrogel–calcium phosphate composite supported the formation of a calcified cartilage-like matrix and is a promising scaffold design for osteochondral interface tissue engineering.

Introduction

Osteoarthritis is the predominant form of arthritis[1] and it remains the leading cause of disability among Americans.[2] Arthritic joints are characterized by lesions in hyaline cartilage that result in severe pain and loss of motion. Hyaline cartilage is essential for articulation of load-bearing joints and serves to absorb shock, distribute load, and facilitate motion.[3] Current treatment options for osteoarthritis include lavage, periosteal grafts, subchondral drilling or microfracture, and mosaicplasty. Many of these techniques, however, result in suboptimal clinical outcome due to donor-site morbidity, poor graft-to-bone fixation, and formation of fibrocartilage instead of articular cartilage postrepair.[4–6]

Alternative cartilage repair approaches focus on tissue-engineered cartilage grafts that have been investigated for the treatment of full-thickness cartilage defects with promising results. A significant challenge remains in how to engineer a consistent and stable osteochondral interface for achieving integrative cartilage repair and osteointegration of the cartilage graft. The native cartilage connects to bone via the osteochondral interface, which consists of a layer of hypertrophic chondrocytes embedded in a mineralized cartilage matrix[7,8] and exhibits an elastic modulus intermediate between uncalcified cartilage and subchondral bone.[9] This calcified cartilage layer allows for functional cartilage-to-bone integration and enables pressurization during physiological loading, while also serving as a barrier against vascular invasion.[10–12] The importance of this barrier between cartilage and bone was demonstrated by Hunziker *et al.* using a full-thickness cartilage defect model.[13] It was observed that a "structural barrier," in this case a Gore-Tex® membrane (0.2 μm pore diameter) placed between the cartilage and bone compartments, was necessary to maintain the integrity of the newly formed cartilage, largely by limiting vascular ingrowth from the subchondral bed and preventing ectopic mineralization.

These observations illustrate that for functional and integrative cartilage repair, it is critical to regenerate a contiguous and stable interface between cartilage grafts and subchondral bone. Published approaches to the formation of the osteochondral interface have largely been cell-based, with chondrocytes cultured in a mineralizing media and/or seeded directly on a calcium phosphate substrate. Kandel *et al.* first seeded deep-zone chondrocytes (DZC) on filter inserts precoated with collagen II and also cultured in a mineralizing media containing 10 mM beta-glycerophosphate.[14] It was found that mineralized matrix was formed in the region directly adjacent to the insert. More recently, Allan *et al.* seeded DZC at high density on porous calcium polyphosphate scaffolds, cultured in mineralization media,[15] and observed that a matrix containing semicrystalline calcium

[1]Biomaterials and Interface Tissue Engineering Laboratory and [2]Liu Ping Laboratory for Functional Tissue Engineering Research, Department of Biomedical Engineering, Columbia University, New York, New York.

phosphate was formed adjacent to the scaffold. These results suggest that DZC represent a promising chondrocyte population for calcified cartilage formation, and the next step is to address the functional requirements of cartilage-to-bone integration by combining cells with scaffolds for osteochondral interface tissue engineering.

A scaffold-based approach is advantageous for osteochondral interface regeneration for several reasons. First, relatively fewer chondrocytes are required than the cell-based approach, and second, functional mechanical properties can be readily achieved with a scaffold system. Moreover, it is possible to preincorporate a biomimetic ceramic phase to further augment scaffold mechanical properties and facilitate the establishment of a functional calcified cartilage matrix. The ideal cartilage-to-bone interface scaffold should support chondrocyte viability and promote the formation of a calcified cartilage matrix with physiologically relevant mechanical properties. Further, the interface scaffold must be osteointegrative.

The focus of this study, guided by these design criteria, is to evaluate the potential of a hydrogel–ceramic composite scaffold to promote chondrocyte-mediated formation of a calcified cartilage-like matrix *in vitro*. The cartilage phase of the scaffold will be based on alginate, a hydrogel comprised of linear chains of covalently linked block-co-polymers of (1,4)-linked β-D-mannuronic acid and α-L-guluronic acid.[16] Alignate has been utilized extensively for chondrocyte culture[17–19] and cartilage tissue engineering.[20–22] Chondrocytes have been shown to maintain their native morphology and deposit a matrix rich in both proteoglycan and collagen in alginate, which also has the advantage of being biocompatible, nonimmunogenic, and biodegradable. Moreover, the ambient gelation conditions associated with alginate have been reported to preserve the bioactivity of growth factors.[23] The ceramic phase of the interface scaffold consists of hydroxyapatite (HA) particles, which is intended to mimic the mineral phase of the calcified cartilage interface.[24,25] Although hydrogel–ceramic scaffolds have not been explored for calcified cartilage regeneration, this type of composite scaffold has been tested for bone applications and shown to promote calcification *in vitro*.[26,27] For example, in a study by Patel *et al.*, nanosized HA particles were incorporated in a cyclic acetal hydrogel with predifferentiated rat bone marrow stromal cells.[28] It was found that HA presence increased cell alkaline phosphatase (ALP) activity and promoted osteogenesis.

The first objective of this study is to determine the response of chondrocytes in the composite alginate–HA scaffold, focusing on changes in cell growth, biosynthesis, and mineralization, as well as scaffold compressive and shear mechanical properties. The second objective of this study is to identify a chondrocyte population that is optimal for calcified cartilage formation. Currently, the majority of cartilage tissue engineering scaffolds are seeded with full-thickness chondrocytes derived from all the three zones of articular cartilage.[29–31] Given the promising results of the aforementioned cell-based approaches to interface tissue engineering, this study will compare the response of DZC, the cells residing in the deep zone of cartilage and directly above the calcified cartilage interface,[32] with that of the commonly used full-thickness chondrocytes. It is hypothesized that the presence of the HA phase within the alginate hydrogel scaffold will promote the formation of a calcified cartilage matrix, and differences in biosynthesis due to cell population are also expected. Findings of this study are anticipated to provide new insights into the design of a biomimetic osteochondral interface scaffold for integrative and functional cartilage repair.

Materials and Methods

Cells and cell culture

Primary articular chondrocytes were isolated from five neonatal calf knees following published protocols, and pooled together for use in this study.[33] Specifically, cells that were digested from the bottom third of articular cartilage were designated as DZC. For comparison, full thickness chondrocytes (FTC) were also isolated. Briefly, the cartilage pieces were digested for 16 h with 0.1 w/v% collagenase (Sigma) in Dulbecco's modified Eagle's medium (DMEM) supplemented with 5% fetal bovine serum (FBS; Atlanta Biologicals), 2% antibiotics (10,000 U/mL penicillin and 10 mg/mL streptomycin), and 0.1% antifungal (amphotericin B). The cell suspension was then sterile filtered before plating (30 μm; Spectrum). The isolated chondrocytes were maintained in high-density culture (4×10^5 cells/cm^2) in fully supplemented DMEM with 10% FBS, 1% nonessential amino acids, 1% antibiotics, and 0.1% antifungal for 48 h before seeding. All media supplements were purchased from Cellgro-Mediatech unless otherwise specified.

Scaffold fabrication, characterization, and culture

Medium viscosity sodium salt alginic acid (Sigma) was used to prepare a 2% alginate solution in phosphate-buffered saline (PBS). A custom mold was used to crosslink the alginate scaffolds (10 mm diameter × 1.6 mm height) with 50 mM $CaCl_2$ (Sigma) and 150 mM NaCl (Sigma) for 30 min.[17] Acellular and cellular alginate scaffolds with 1.5 wt/v% HA (20 μm; Sigma) and the corresponding samples without HA were fabricated. The experimental group consisted of cells in alginate scaffolds with HA (Alg + HA), whereas the control groups include cells in alginate (Alg), as well as corresponding acellular controls for alginate and alginate + HA groups. To form the cell-seeded scaffolds, chondrocytes were mixed into the alginate solution (1×10^7 cells/mL) before crosslinking. All samples were cultured under humidified conditions at 37°C and 5% CO_2, and maintained in ITS media composed of DMEM supplemented with 1% ITS+ Premix (BD Biosciences), 1% antibiotics, 0.1% antifungal, and 40 μg/mL proline (Sigma). The media were changed every other day and freshly supplemented with 50 μg/mL ascorbic acid (Sigma). In this study, chondrocyte response in the alginate + HA scaffolds was evaluated over 4 weeks of culture. Specifically, cell viability, proliferation, collagen and glycosaminoglycan (GAG) deposition, scaffold mechanical properties, mineralization, and hypertrophy were determined and compared between groups as well as over time.

Distribution of HA ($n=2$) in the as-fabricated acellular and cellular alginate + HA scaffolds was visualized by environmental scanning electron microscopy (ESEM, 15 kV; JEOL 5600LV), and elemental composition was ascertained using energy dispersive X-ray analysis (EDAX, 15 kV, FEI Quanta 600; FEI Co.). In addition, samples were weighed and

desiccated for 24 h (CentriVap Concentrator; Labconco Co.), after which the scaffold swelling ratio ($n=4$, wet weight/dry weight) and water content ($n=4$, water weight/wet weight) were calculated.

Cell proliferation and viability

Cell viability ($n=2$) was visualized using Live/Dead staining (Molecular Probes), following the manufacturer's suggested protocol. After washing in PBS, samples were imaged under confocal microscopy (Olympus Fluoview IX70) at excitation and emission wavelengths of 488 nm and 568 nm, respectively. Cell proliferation ($n=5$) was determined using the PicoGreen® total DNA assay (Molecular Probes). Briefly, the samples were first rinsed with PBS, and 300 μL of 0.1% Triton-X solution (Sigma) was used to lyse the cells. An aliquot of the sample (25 μL) was then added to 175 μL of the PicoGreen working solution. Fluorescence was measured with a microplate reader (Tecan), at the excitation and emission wavelengths of 485 nm and 535 nm, respectively. Total cell number was obtained by converting the amount of DNA per sample to cell number using the conversion factor of 7.7 pg DNA/cell.[34]

Cell size was determined by labeling the cells with the membrane dye calcein AM and imaging the samples under confocal microscopy at excitation and emission wavelengths of 488 and 568 nm, respectively (Olympus Fluoview IX70). Three representative images were taken for each experimental group, with seven cells analyzed per image using ImageJ (National Institute of Health), and both cell cross-sectional area ($n=21$) and aspect ratio ($n=21$) were calculated.

Matrix deposition

Collagen deposition ($n=5$) was quantified using the Sircol assay (Biocolor) according to the manufacturer's suggested protocol, which detects type I-V collagen.[35] Bovine collagen I solution (Biocolor) was used as a standard. Briefly, the samples were first desiccated for 24 h and then digested for 16 h at 60°C with papain (600 mg protein/mL) in 0.1 M sodium acetate (Sigma), 10 mM cysteine HCl (Sigma), and 50 mM ethylenediaminetetraacetate (Sigma). Absorbance was measured at 555 nm using a microplate reader (Tecan). Additionally, collagen distribution ($n=2$) was visualized by Picrosirius red staining. Briefly, the samples were first fixed in neutral buffered formalin and 1% cetylpyridinium chloride (Sigma) for 24 h, followed by dehydration with an ethanol series. The dehydrated samples were embedded in paraffin (Type 9, Richard-Allan Scientific, Kalamazoo, MI), sectioned from the center of the scaffold (7 μm slices), and mounted on microscope slides, before staining and imaging.

Overall matrix deposition and cellularity was determined with H&E staining ($n=2$). Deposition of types I, II, and X collagen ($n=2$) in the alginate and alginate + HA scaffolds was evaluated using immunohistochemistry. Monoclonal antibodies for type I collagen (1:20 dilution) and type II collagen (1:100) were obtained from Abcam, and type X collagen antibody (1:1) was obtained from the Developmental Studies Hybridoma Bank (University of Iowa). After fixation, samples were treated with 1% hyaluronidase for 30 min at 37°C and incubated with primary antibody overnight. An FITC-conjugated secondary antibody (LSAB2; Abcam) was added and the sections were imaged under confocal microscopy at excitation and emission wavelengths of 488 and 568 nm, respectively.

Sample GAG content ($n=5$) was determined with a modified 1,9-dimethylmethylene blue (DMMB) binding assay,[36–38] with chondroitin-6-sulfate (Sigma) as the standard. To account for the anionic nature of the carboxyl groups on the alginate hydrogel, the pH of the DMMB dye solution was adjusted to 1.5 with concentrated formic acid (Sigma) so that only the sulfated GAG-DMMB complexes were detectable. Additionally, the absorbance difference between 540 nm and 595 nm was used to improve the sensitivity in signal detection. Proteoglycan distribution ($n=2$) was visualized histologically with Alcian blue staining of paraffin-embedded sections.[34]

Scaffold mechanical properties

Scaffold mechanical properties ($n=3$) were determined following published protocols.[39] Briefly, scaffold diameter (d) was measured with a stereomicroscope (Bausch and Lomb) and testing was performed on a shear-strain controlled rheometer (TA instruments). Each sample was placed between two flat porous platens and immersed in DMEM to prevent dehydration. The equilibrium compressive Young's modulus (E_{eq}) of the sample was calculated at 15% compressive strain (ε) as follows:

$$\mathrm{E_{eq}} = \frac{\sigma}{\varepsilon} \text{ where } \sigma = \frac{\Delta F}{\pi d^2/4}, \quad (1)$$

Where, ΔF is the change in equilibrium normal force due to the axial compression. The 15% compressive strain chosen here is within the physiological range for articular cartilage.[40] Finally, a dynamic shear test was performed (0.01–10 Hz) with a logarithmic frequency sweep at a shear strain of 0.01 radian. The complex shear modulus was calculated as follows:

$$G^* = \frac{Td}{2I_p\gamma}, \quad (2)$$

Where, γ is the sinusoidal shear strain and T is the torque response. In general, G^* is a complex number and can be expressed as $G^* = G' + iG''$. The magnitude of the complex shear modulus ($|G^*|$) is therefore given by $|G^*| = \sqrt{(G')^2 + (G'')^2}$, and the phase shift angle (δ) between the applied strain and the torque response could be calculated from $\delta = \tan^{-1}(G''/G')$.

Mineralization

Mineralization potential was determined by measuring ALP activity ($n=5$) using an colorimetric assay based on the hydrolysis of *p*-nitrophenyl phosphate (*p*NP-PO_4) to *p*-nitrophenol (pNP).[41] Briefly, the samples were lysed in 0.1% Triton-X solution, then added to *p*NP-PO_4 solution (Sigma) and allowed to react for 30 min at 37°C. The reaction was terminated with 0.1 N NaOH (Sigma), and sample absorbance was measured at 415 nm using a microplate reader (Tecan). In addition, mineral distribution ($n=2$) was evaluated by von Kossa staining with 5% silver nitrate, followed by 30 min of UV exposure.[42] Additionally, media calcium

concentrations ($n=5$) were quantified using the Arsenazo III dye (Pointe Scientific), with absorbance measured at 620 nm using a microplate reader.[43]

Chondrocyte hypertrophy

The expression of hypertrophic markers, such as matrix metalloproteinase-13 (MMP-13), RUNX-2, and type X collagen ($n=3$), were measured using reverse transcription followed by polymerase chain reaction. The oligonucleotide primer sequences were as follows: β-actin: CTGCGGCATTCACGAAACTA (sense), ACCGTGTTGGCGTAGAGGTC (antisense); MMP-13: ACATCCCAAAACGCCAGACAA (sense), GATGCAGCCGCCAGAAGAAT (antisense); RUNX-2: AATCCTCCCCAAGTTGCCA (sense), RUNX-2: TTCTGTC TGTCCTTCTGGGT (antisense); type X collagen: TGGATC CAAAGGCGATGTG (sense), GCCCAGTAGGTCCATTAA GGC (antisense). Total RNA was isolated using the TRIzol (Invitrogen) extraction method, with the isolated RNA reverse-transcribed into cDNA using the SuperScript III First-Strand Synthesis System (Invitrogen). The cDNA product was then amplified for 35 cycles with recombinant Platinum Taq DNA polymerase (Invitrogen). Expression band intensities of relevant genes were analyzed semiquantitatively and normalized to the housekeeping gene β-actin.

Statistical analysis

Results are presented in the form of mean ± standard deviation, with n equal to the number of samples analyzed. A two-way analysis of variance was performed to determine the effects of mineral presence and culturing time on cell response (proliferation, matrix deposition, ALP activity, solution calcium concentration, gene expression, or cell size), as well as scaffold parameters (weight, thickness, swelling ratio, or mechanical properties). The Tukey–Kramer *post hoc* test was used for all pairwise comparisons, and significance was attained at $p<0.05$. All statistical analyses were performed using JMP 4.0.4 (SAS Institute).

Additionally, linear regression analysis of the correlation between mechanical properties and matrix deposition was performed. Specifically, mechanical properties and matrix content (GAG and collagen) from the cell-seeded alginate and alginate + HA groups ($n=6$/group) were correlated at both day 14 and 28 (R^2, slope, and p-value). It is well established that the mechanical properties of cartilage are related to collagen and GAG content.[44,45] Therefore, the correlation between mechanical properties (E_{eq} and $|G^*|$) and scaffold collagen and GAG content was determined both individually (GAG or Col) and in combination (GAG + Col), using linear regression models.

Results

Acellular scaffold characterization

Acellular alginate and alginate + HA scaffolds were visualized with environmental scanning electron microscopy (Fig. 1A). The alginate scaffold was homogeneous and uniform in appearance. Whereas in the alginate + HA scaffold,

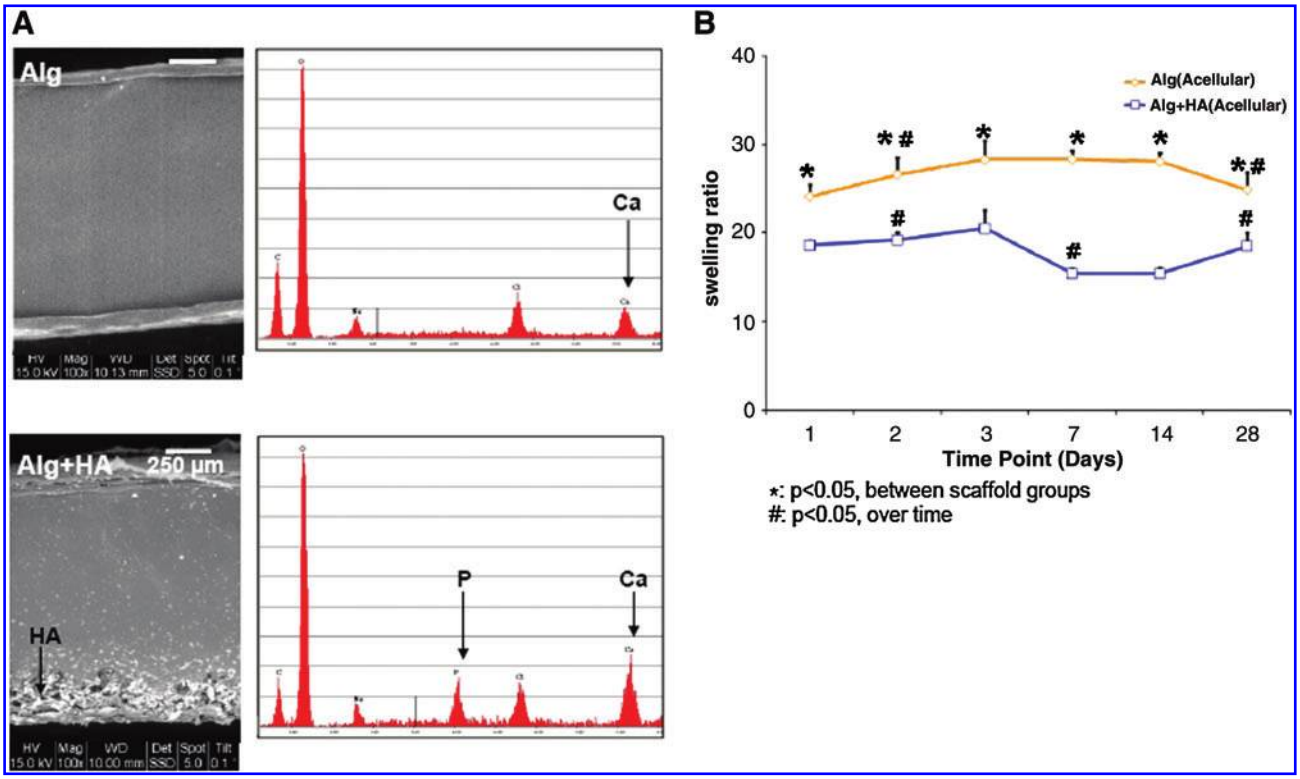

FIG. 1. Acellular scaffold characterization. **(A)** Hydrogel scaffolds were visualized with environmental electron microscopy (15 kV, 100×, day 1, bar = 250 um, $n=2$). Energy-dispersive X-ray analysis confirmed the presence of phosphorus (P) in the alginate + HA scaffolds. **(B)** At all time points examined, the swelling ratio of the alginate + HA group was lower than that of the alginate group (*$p<0.05$, $n=4$). HA, hydroxyapatite. Color images available online at www.liebertonline.com/tea

HA was distributed throughout the scaffold; aggregation of HA particles was observed at the bottom of the scaffold. EDAX confirmed the presence of sodium (Na), chlorine (Cl), and calcium (Ca) in both the alginate and alginate + HA scaffolds as a result of the sodium-alginic salt and divalent Ca^{+2} cross-linking reaction (Fig. 1A). The presence of the phosphorus (P) peak was only detected in the alginate + HA scaffolds, accompanied by elevated peak intensity for Ca (Fig. 1A).

Both acellular alginate and alginate + HA scaffolds exhibited changes in swelling ratio over time (Fig. 1B), with a significant increase detected during the first 24 h of culture. Thereafter, swelling of the alginate group remained unchanged until a significant decrease was observed after 3 weeks of culture, which was most likely related to scaffold degradation. In contrast, the swelling ratio of the alginate + HA group increased significantly by day 28. It is noted that at all time points examined, the swelling ratio of the alginate + HA group remained significantly lower than that of the alginate group.

Cellular scaffold characterization

The cell-seeded alginate and alginate + HA scaffolds measured significantly higher wet weight as compared with their corresponding acellular controls at day 14 and 28 (Table 1). While there was no change in wet weight of the acellular scaffolds from day 1 to 14, a significant increase was found over the first 2 weeks of culture in the cell-laden scaffolds. No significant difference in wet weight was detected between the cellular alginate and alginate + HA groups. The cell-seeded scaffolds measured a significantly larger diameter as compared with their corresponding acellular controls at day 28 (Table 1), and again, no difference was found between chondrocyte-laden alginate and alginate + HA groups. Both types of scaffolds were significantly thicker as compared with their corresponding acellular controls at day 14 (Table 1). Further, a greater scaffold thickness was measured for the alginate + HA group as compared with the alginate group at day 28 ($p < 0.05$).

Cell growth and extracellular matrix deposition

Chondrocytes remained viable over time (Fig. 2A) and were spherical in shape in the alginate scaffolds. Similar to the published studies of chondrocytes cultured in alginate,[39] cell number decreased initially and stabilized thereafter (Fig. 2B). Interestingly, a significantly higher number of cells was found on the alginate + HA scaffolds as compared with the alginate control from day 7 to 28.

Matrix deposition was uniformly distributed throughout the depth of the scaffolds (Fig. 2A). Collagen production increased in both types of scaffolds over time, with the alginate + HA group measuring significantly higher collagen content than the alginate control at day 28 (Fig. 3A). To account for differences in cell number between alginate and alginate + HA scaffolds, collagen content was also normalized to scaffold DNA content. It was found that collagen deposition per cell was 30% higher in alginate + HA scaffolds. These results were confirmed by histological staining (Fig. 3C). No positive staining was seen for type I collagen in either of the scaffold type, whereas type II collagen staining was present in alginate scaffolds and strongly positive for cells cultured in the alginate + HA group. While proteoglycan deposition increased over time for both scaffold groups, no significant difference between scaffold types was observed (Fig. 3B). At day 14, GAG deposition per cell was significantly lower in the HA-containing scaffolds, but this difference was not observed at day 28. Histological analysis revealed that GAG deposition was evident throughout all scaffolds, with localization of matrix deposition clustered around individual chondrocytes (Fig. 3C).

Structure–function relationship

The mechanical properties of both acellular and cell-seeded alginate and alginate + HA scaffolds were assessed under unconfined compression and dynamic shear. The cell-seeded groups consistently exhibited higher shear modulus and phase shift angle as compared with their respective acellular controls after 2 weeks of culture (Fig. 4, $p < 0.05$). In general, a high phase shift angle (i.e., $\delta \to 90°$) represents a highly viscous material, while a low value ($\delta \to 0°$) indicates minimal internal energy damping in a material, with $\delta = 0°$ defining an elastic material (i.e., no energy dissipation). Further, the cell-seeded alginate + HA scaffolds measured significantly higher shear modulus and phase shift angle than the alginate scaffolds at day 28 (Fig. 4).

To investigate the relationship between matrix deposition and scaffold mechanical properties, normalized matrix content (GAG or collagen/wet weight) was systematically correlated with mechanical properties. For the alginate group,

Table 1. Scaffold Properties

		Wet weight (mg)		*Thickness (mm)*		*Diameter (mm)*	
		Acellular	*DZC-seeded*	*Acellular*	*DZC-seeded*	*Acellular*	*DZC-seeded*
Day 1	Alg	147.5 ± 6.6	141.2 ± 4.6	1.779 ± 0.023	1.859 ± 0.097	9.698 ± 0.065	9.752 ± 0.061
	Alg + HA	149.6 ± 2.4	143.9 ± 1.0	1.841 ± 0.029^{a}	1.849 ± 0.057	9.690 ± 0.063	9.771 ± 0.029
Day 14	Alg	143.5 ± 6.9	$167.4 \pm 5.4^{b,c}$	1.440 ± 0.036^{b}	1.868 ± 0.001^{c}	9.809 ± 0.041^{b}	9.849 ± 0.028^{b}
	Alg + HA	140.9 ± 4.4	$161.5 \pm 6.9^{b,c}$	$1.640 \pm 0.092^{a,b}$	1.850 ± 0.039^{c}	9.832 ± 0.056^{b}	9.871 ± 0.022^{b}
Day 28	Alg	126.0 ± 9.0^{b}	174.1 ± 7.3^{c}	1.667 ± 0.042^{b}	1.799 ± 0.008^{b}	9.642 ± 0.092^{b}	9.891 ± 0.047^{c}
	Alg + HA	137.6 ± 11.2	167.4 ± 4.0^{c}	$1.803 \pm 0.088^{a,b}$	$1.893 \pm 0.033^{a,b}$	9.643 ± 0.055^{b}	9.812 ± 0.114^{c}

Cell culture resulted in higher wet weight, larger scaffold diameter, and thickness as compared with corresponding acellular controls ($^{c}p < 0.05$, $n = 4$). Alginate + HA scaffolds were significantly thicker than the alginate scaffolds by day 28 ($^{a}p < 0.05$), with no difference in wet weight or diameter observed between the cell-seeded groups. HA, hydroxyapatite; DZC, deep zone chondrocytes.

$^{a}p < 0.05$, between scaffold groups, within acellular or cell-seeded samples.

$^{b}p < 0.05$, over time.

$^{c}p < 0.05$, between corresponding acellular and cell-seeded scaffold groups.

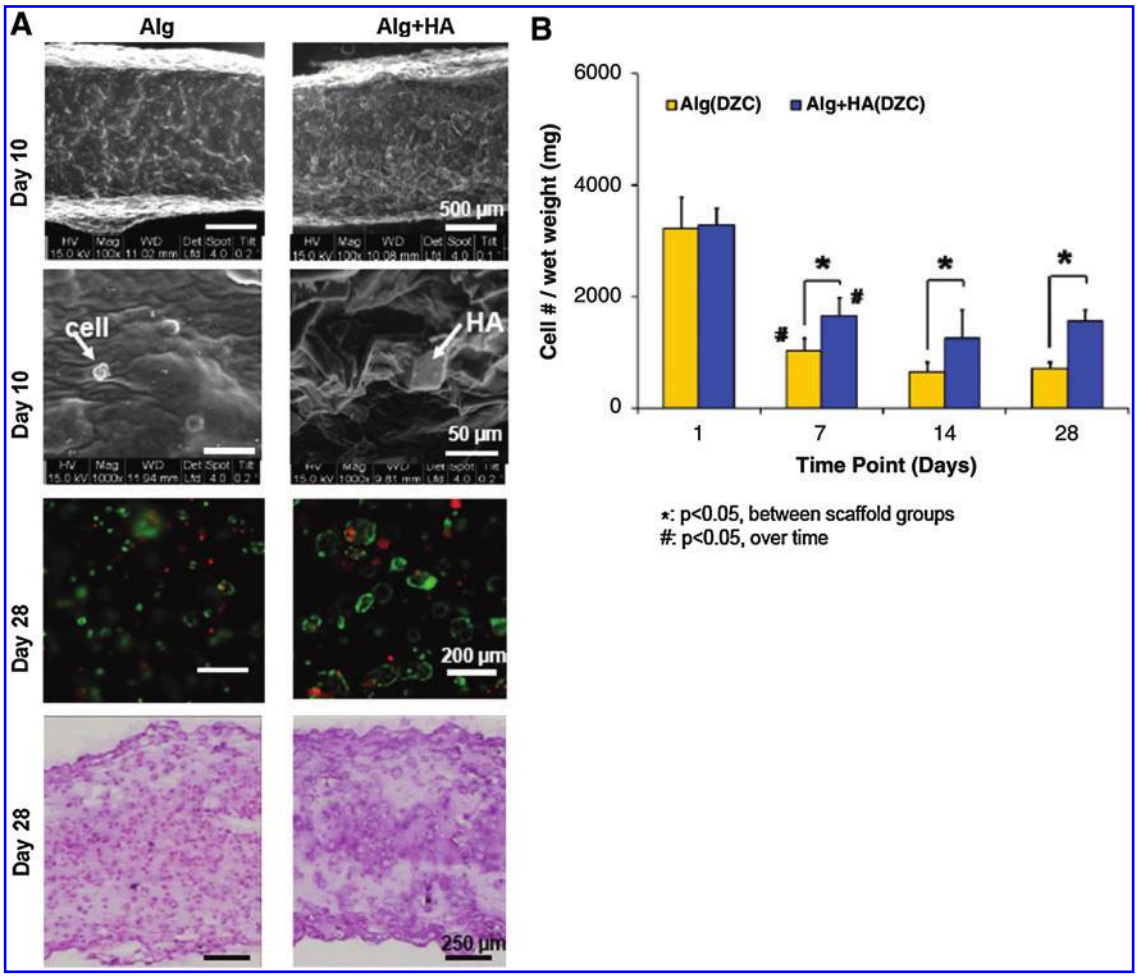

FIG. 2. Cell viability, morphology, and growth. **(A)** Scaffolds maintain their integrity over time (15 kV, 100×, bar = 500 um, n = 2), and individual cells and HA particles are observed within the hydrogel (1000×, bar = 50 um). Chondrocytes remained viable over time in the hydrogel scaffolds (10×, bar = 200 um, $n = 2$), with uniform matrix deposition throughout the scaffold (H&E, 5×, bar = 250 um, $n = 2$). **(B)** Cell number decreased from day 1 to 7, and remained unchanged thereafter ($^{\#}p < 0.05$, $n = 5$). A higher number of cells was consistently found on the alginate + HA scaffolds as compared with the alginate control ($^{*}p < 0.05$). Color images available online at www.liebertonline.com/tea

mechanical properties did not correlate with either GAG or collagen. Similarly for the alginate + HA group, no significant correlation was found between matrix components and either compressive modulus or phase shift angle. However, when matrix contents (collagen and GAG) were individually correlated with shear modulus (G^*) for the alginate + HA group, a positive linear correlation with either GAG ($R^2 = 0.79$, Fig. 5A) or collagen content ($R^2 = 0.84$, Fig. 5B) was detected. Further, when the matrix components were both correlated with mechanical properties (GAG + Col), the coefficient of determination between total matrix content and shear modulus increased to 0.89 ($p < 0.05$, Table 2).

Mineralization and hypertrophy

Chondrocyte ALP activity was evident in both alginate and alginate + HA scaffolds, although a significant temporal decrease in activity was observed in both groups. At day 7, ALP activity decreased significantly in the alginate + HA group as compared with the alginate group, although by day 28, cells in the alginate + HA group measured a higher ALP activity (Fig. 6A, $p < 0.05$). Media calcium was significantly lower for the alginate + HA group as compared with the alginate control and plain media at day 14 (Fig. 6B). In contrast, media for the acellular alginate + HA and alginate groups did not differ from plain media. Mineral deposition visualized by von Kossa confirmed the distribution of HA particles in the alginate + HA scaffold observed by ESEM (Fig. 6C). By day 28, positive von Kossa staining was detected in the matrix surrounding chondrocytes.

In terms of cell size, the average chondrocyte cross-sectional area was found to be $1164 \pm 541\ \mu m^2$ in the alginate control at day 28 (Fig. 7A). In contrast, cells cultured in alginate + HA scaffolds measured a cross-sectional area of $2927 \pm 823\ \mu m^2$ at day 28, representing a 250% increase as compared with the alginate control ($p < 0.05$). Expression of MMP-13 was detected in both scaffold groups, with a significant downregulation observed from day 14 to 28 in the alginate + HA group (Fig. 7B). At day 14, MMP-13 expression was significantly higher for the alginate + HA group as compared with the alginate group. Runx-2 expression decreased over time, with no difference observed between groups (data not shown). While minimal

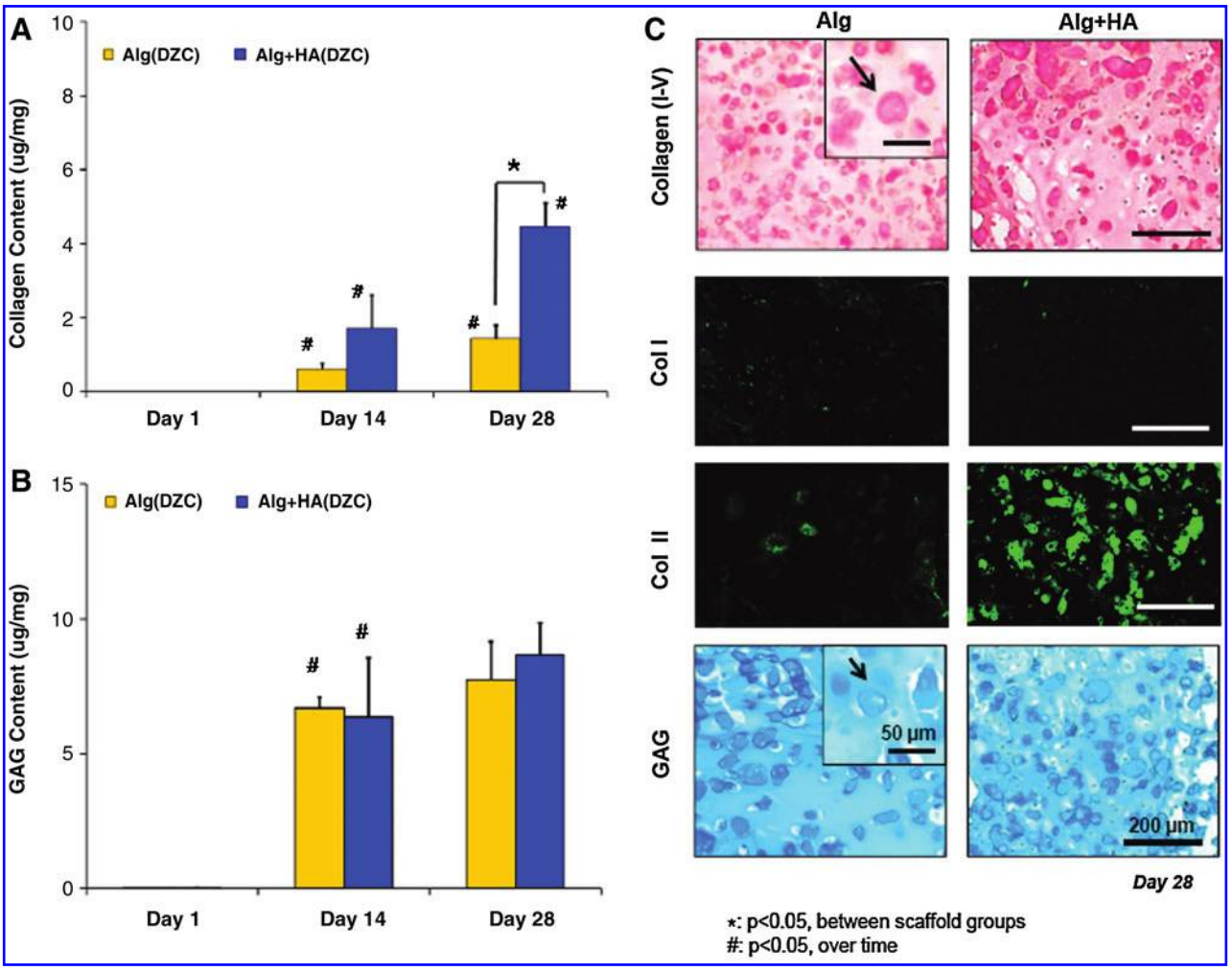

FIG. 3. Extracellular matrix deposition. **(A)** Collagen production increased in both types of scaffolds over time ($^{\#}p<0.05$, $n=5$), with the alginate+HA group measuring significantly higher collagen content than the alginate control by day 28 ($^{*}p<0.05$). **(B)** While proteoglycan deposition increased over time for both scaffold groups ($^{\#}p<0.05$, $n=5$), no significant difference between the groups was observed. **(C)** Corresponding histology for collagen and GAG shows positive staining (10×, bar=200 um, $n=2$) and pericellular matrix deposition (inset: 20×, bar=50 um, $n=2$). While there was minimal staining for type I collagen in both groups, there was strong positive type II collagen staining evident for the alginate+HA group at day 28 (10×, bar=200 um, $n=2$). Color images available online at www.liebertonline.com/tea

type X collagen expression and deposition was observed in the alginate group, it was upregulated for the alginate+HA group over time (Fig. 7C, $p<0.05$). In addition, type X collagen expression in the alginate+HA group was significantly higher than that of the alginate control and corresponded with strongly positive type X collagen staining.

Effect of chondrocyte population

Both matrix deposition and mineralization potential of DZC in alginate and alginate+HA scaffold were also compared with those of full-thickness chondrocytes (FTC) collected from all the three layers of articular cartilage (surface, middle, and deep). In terms of biosynthesis, no significant difference in total collagen content was observed between DZC and FTC when cultured in the alginate control. However, in the alginate+HA scaffold, significantly higher collagen deposition was evident for the DZC group at day 28 as compared with the FTC group (Fig. 8A). Proteoglycan deposition in alginate scaffolds was significantly higher for the DZC versus the FTC group (Fig. 8B, $p<0.05$). Similarly, in the alginate+HA scaffolds, higher proteoglycan deposition was also measured for the DZC group ($p<0.05$).

In terms of mineralization potential, as expected, DZC exhibited significantly higher ALP activity than FTC when cultured in alginate scaffolds for all time points tested. While DZC cultured in alginate+HA measured significantly higher ALP activity as compared with FTC at day 1, no significant difference between these groups was detected thereafter (Fig. 8C). By day 28, type X collagen expression was at basal levels for both DZC and FTC in alginate scaffolds. However, in the alginate+HA scaffolds, significantly higher type X collagen expression was evident for the DZC group as compared with the FTC group (Fig. 8D).

Discussion

The objective of this study is to evaluate the potential of a composite alginate+HA scaffold for osteochondral interface

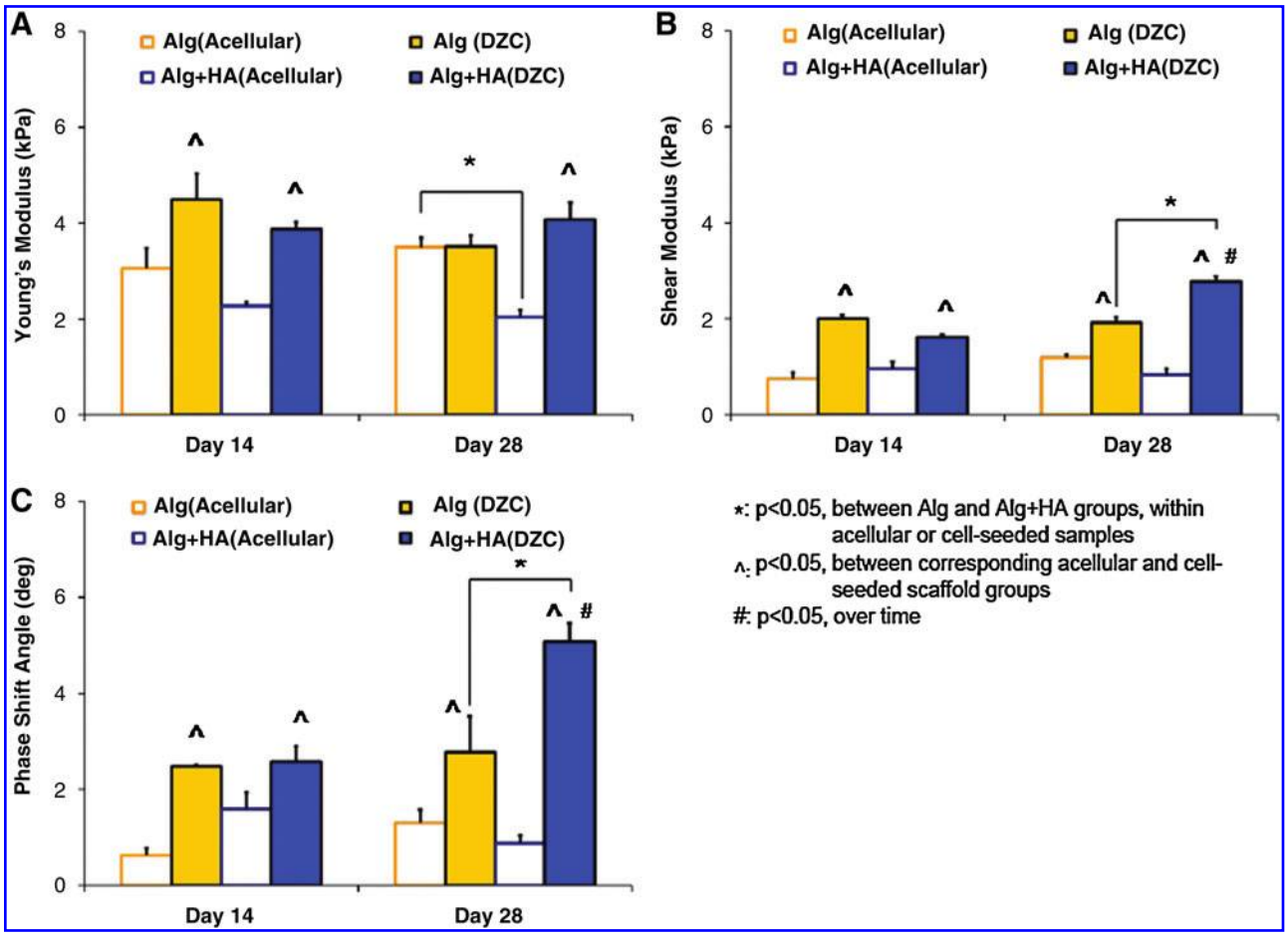

FIG. 4. Mechanical properties. The compressive modulus **(A)**, magnitude of the complex shear modulus **(B)**, and phase shift angle **(C)** of both acellular and DZC-seeded scaffolds were determined. The cell-seeded groups consistently exhibited higher shear modulus and phase shift angle as compared with their respective acellular controls ($\hat{}p < 0.05$, $n = 3$). Moreover, by day 28, both a higher shear modulus and phase shift angle were found in the alginate + HA scaffolds as compared with the alginate control ($*p < 0.05$). DZC, deep-zone chondrocytes. Color images available online at www.liebertonline.com/tea

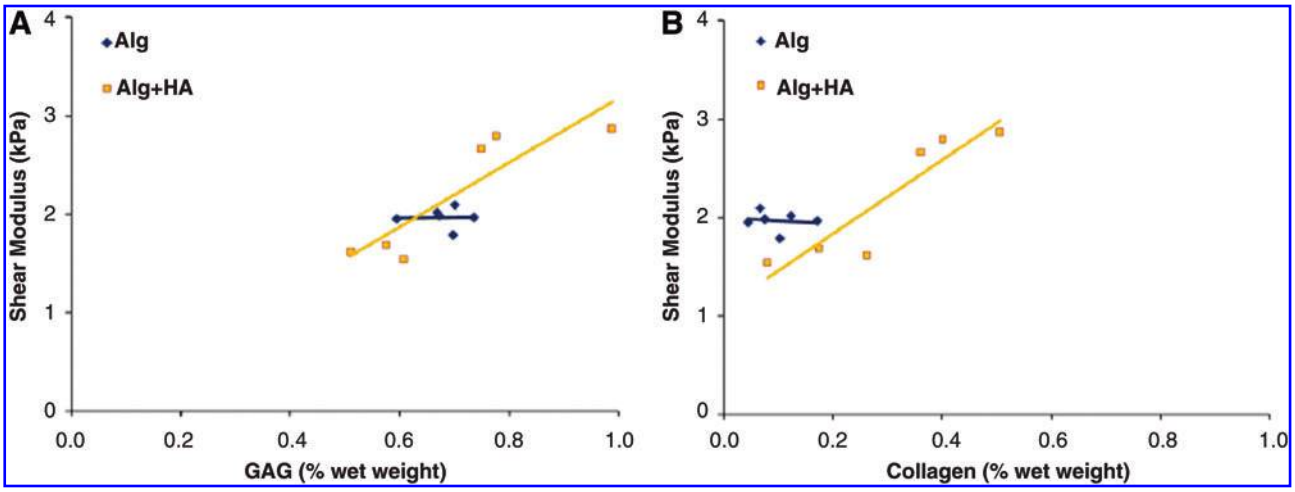

FIG. 5. Structure–function correlation between matrix content and scaffold mechanical properties. A positive correlation between shear modulus and **(A)** glycosaminoglycan (GAG), as well as **(B)** collagen (Col) content, was identified for the alginate + HA group ($n = 6$, R2 = 0.79 for A) GAG, R2 = 0.94 for B) Col, $*p < 0.05$). Color images available online at www.liebertonline.com/tea

Table 2. Structure–Function Correlation

		GAG vs. G[a]	*Col vs. G*[a]	*(GAG + Col) vs. G*[a]
Alg	Slope	—	—	—
	R^2	0.00	0.02	0.04
	p-value	0.99	0.80	0.94
Alg + HA	Slope	3.28	3.76	1.54, 2.43
	R^2	0.79	0.84	0.89
	p-value	0.02[a]	0.01[a]	0.04[a]

A positive correlation between shear modulus and glycosaminoglycan (GAG), as well as collagen (Col) content, was identified for the alginate + HA group ($^{a}p < 0.05$). Further, the coefficient of determination between matrix content and shear modulus increased when both GAG and collagen are correlated with mechanical properties (GAG + Col).

regeneration or, more specifically, for the formation of a calcified cartilage matrix. To this end, the response of DZC in alginate scaffolds with and without HA was determined over time and compared with those of full-thickness chondrocytes. It was found that chondrocytes deposited a well-distributed proteoglycan- and collagen-rich matrix in alginate scaffolds. Interestingly, DZC cultured in alginate + HA scaffolds exhibited elevated collagen deposition, resulting in higher compressive and shear mechanical properties than the ceramic-free alginate control. Despite lower ALP activity, DZC in the composite scaffold were found to be hypertrophic, with significantly greater cell size, as well as upregulated expression of MMP-13 and type X collagen deposition. Moreover, these observed effects were chondrocyte population dependent, as enhanced collagen deposition and hypertrophy was only observed for DZC and not when cells from all three zones of cartilage were cultured

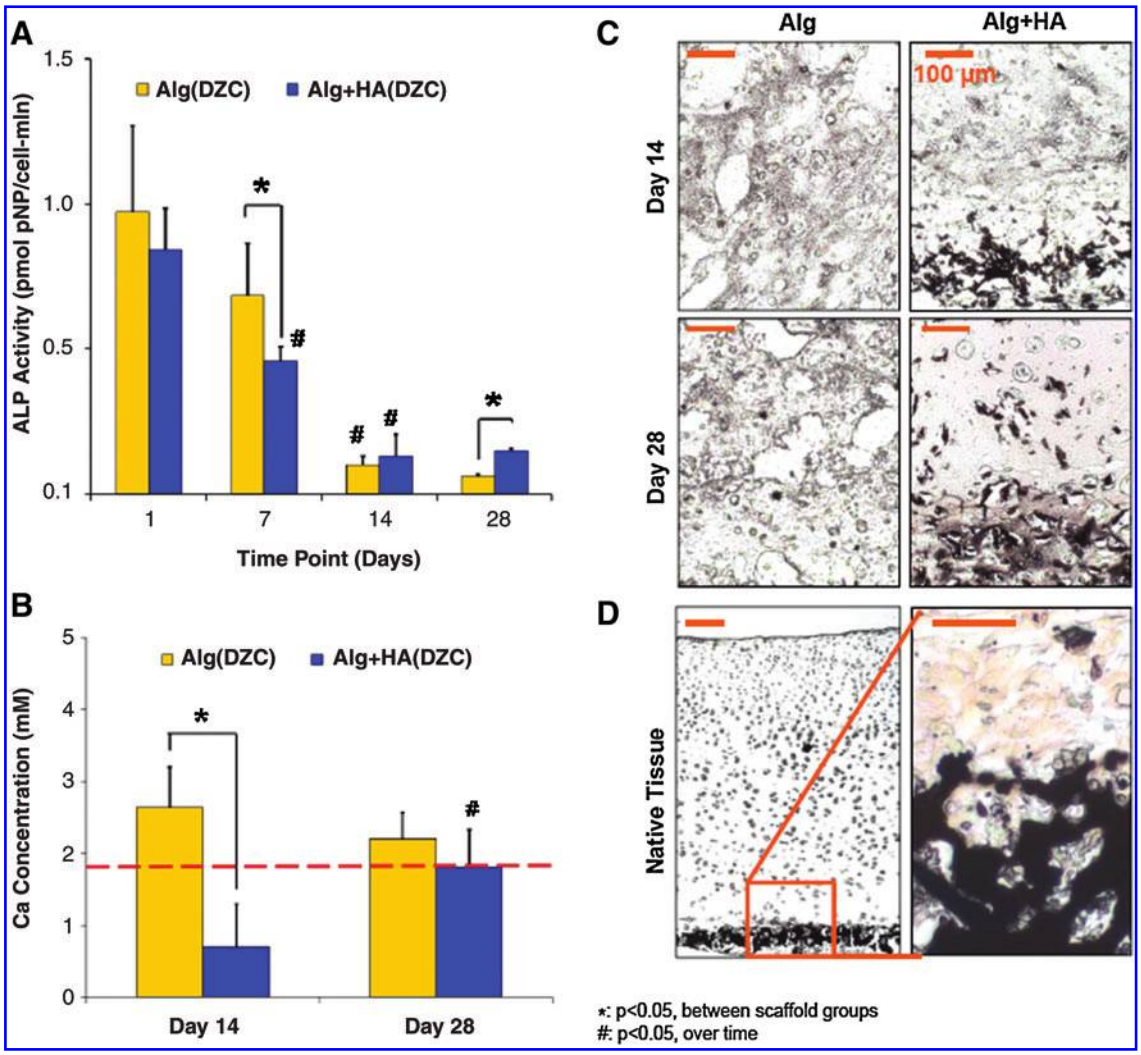

FIG. 6. Mineralization potential and mineral distribution. **(A)** Cell ALP activity decreased over time in both scaffold groups ($^{\#}p < 0.05$, $n = 5$). At day 7, a significantly lower ALP activity was found in the alginate + HA group, although by day 28, the alginate + HA group measured a higher ALP activity than the alginate group ($^{*}p < 0.05$). **(B)** Alginate + HA scaffolds measured a lower media [Ca] at day 14 as compared with the alginate control ($^{*}p < 0.05$, $n = 5$). **(C)** In addition to preincorporated HA, a mineralized matrix was only observed in the alginate + HA group (10×, bar = 100 um, $n = 2$). **(D)** Comparison to von Kossa staining at the native osteochondral interface (5×, bar = 100 um, von Kossa, $n = 2$). ALP, alkaline phosphatase. Color images available online at www.liebertonline.com/tea

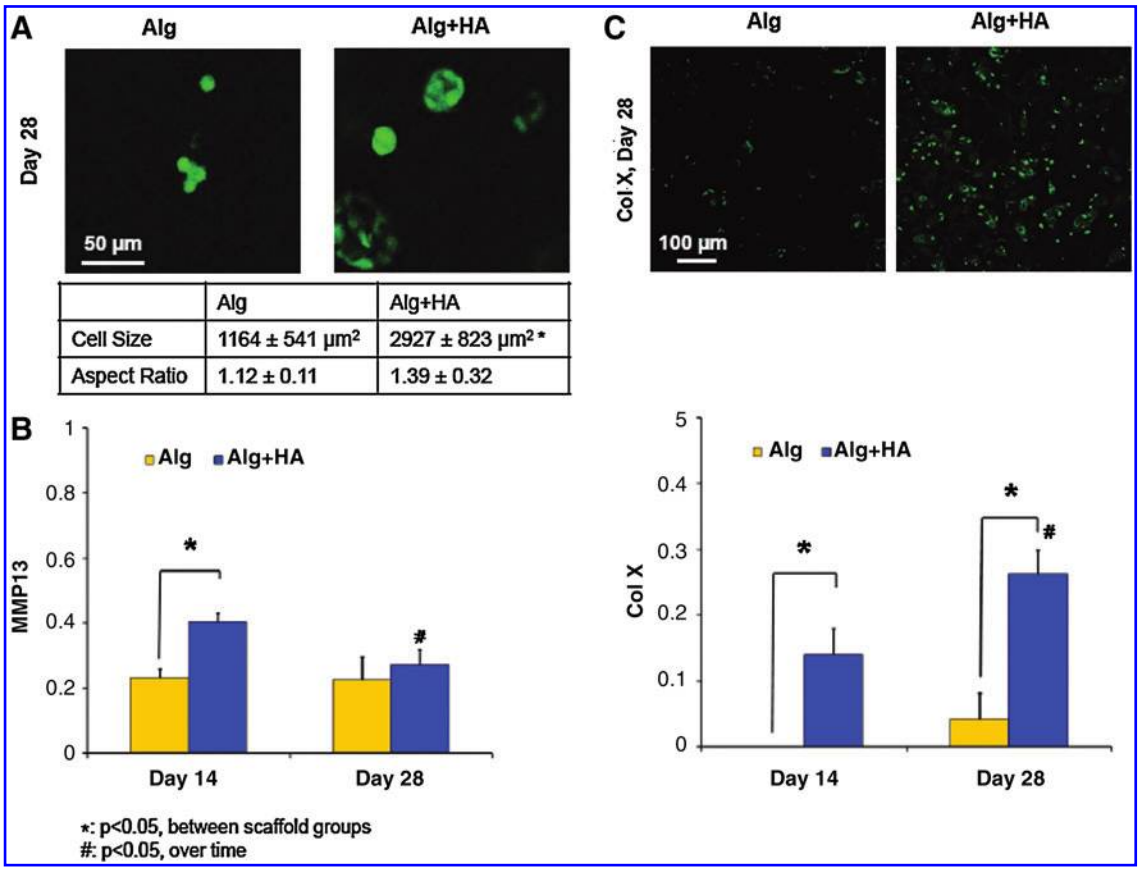

FIG. 7. Chondrocyte hypertrophy. **(A)** Cells in the alginate + HA scaffolds measured a larger cross-sectional area than those in the alginate control (*$p < 0.05$, 32×, bar = 50 um, $n = 20$), with no change found in cell aspect ratio. Expression of hypertrophic markers such as **(B)** MMP-13 and **(C)** type X collagen was significantly higher in the alginate + HA group at day 14 (*$p < 0.05$, $n = 3$), and the upregulation of type X collagen persisted at day 28 with strong positive staining. Type X collagen staining was positive only for the alginate + HA group at day 28 (10×, bar = 100 um, $n = 2$). Color images available online at www.liebertonline.com/tea

together in this scaffold system. Collectively, the results of this study demonstrate that a composite alginate + HA hydrogel scaffold seeded with DZC supports the formation of a calcified cartilage-like matrix.

It was observed here that while the addition of HA to alginate had no effect on total proteoglycan deposition, it resulted in hypertrophy and significant increases in collagen synthesis by DZC. On the other hand, the presence of HA tempers GAG production while simultaneously enhancing collagen deposition by individual chondrocytes. This is not unexpected as decreased proteoglycan content, and specifically loss of large proteoglycan aggregates, has been reported during cartilage mineralization.[46] Both chondrocyte hypertrophy and elevated collagen deposition are also suggestive of calcified cartilage matrix formation, since it has been postulated that collagen allows for aggregation of mineral crystals as well as organized crystal growth and mineral deposition by hypertrophic chondrocytes.[24] In this study, both matrix elaboration and scaffold degradation contributed to changes in mechanical properties over time. As expected for an ionotropic gel such as alginate, degradation occurs as a result of decrosslinking, as evidenced by the lower wet weight found in the acellular scaffolds by day 28.[47] However, in the cell-laden alginate and alginate + HA scaffolds, matrix deposition compensated for hydrogel degradation and resulted in significantly higher shear mechanical properties.[17]

More specifically, higher matrix synthesis by DZC cultured in alginate + HA scaffolds resulted in significantly greater shear modulus and phase shift angle by day 28. While no structure–function relationship was evident in the correlation analysis for the alginate scaffolds, scaffold shear modulus was found to correlate positively with matrix deposition in the alginate + HA scaffolds. Further, there was an increase in the magnitude of the correlation coefficient when both proteoglycan and collagen were related to the shear modulus, suggesting the formation of a functional cartilage matrix.[44,45] It is noted that while the resulting scaffold mechanical properties in this study were only a fraction of those of the native calcified cartilage interface,[48] the positive correlations between cell-mediated matrix deposition and scaffold mechanical properties demonstrate the potential regeneration of both biomimetic and functional tissue in the hydrogel–ceramic composite scaffold. While the mechanical properties of the alginate + HA scaffold do not yet meet those of calcified cartilage,[9] both scaffold (e.g., HA content) and culturing conditions (e.g., mechanical loading) can be optimized to increase its mechanical properties in future studies.

In this study, it was observed that DZC seeded in alginate + HA scaffolds became hypertrophic, as evident by the

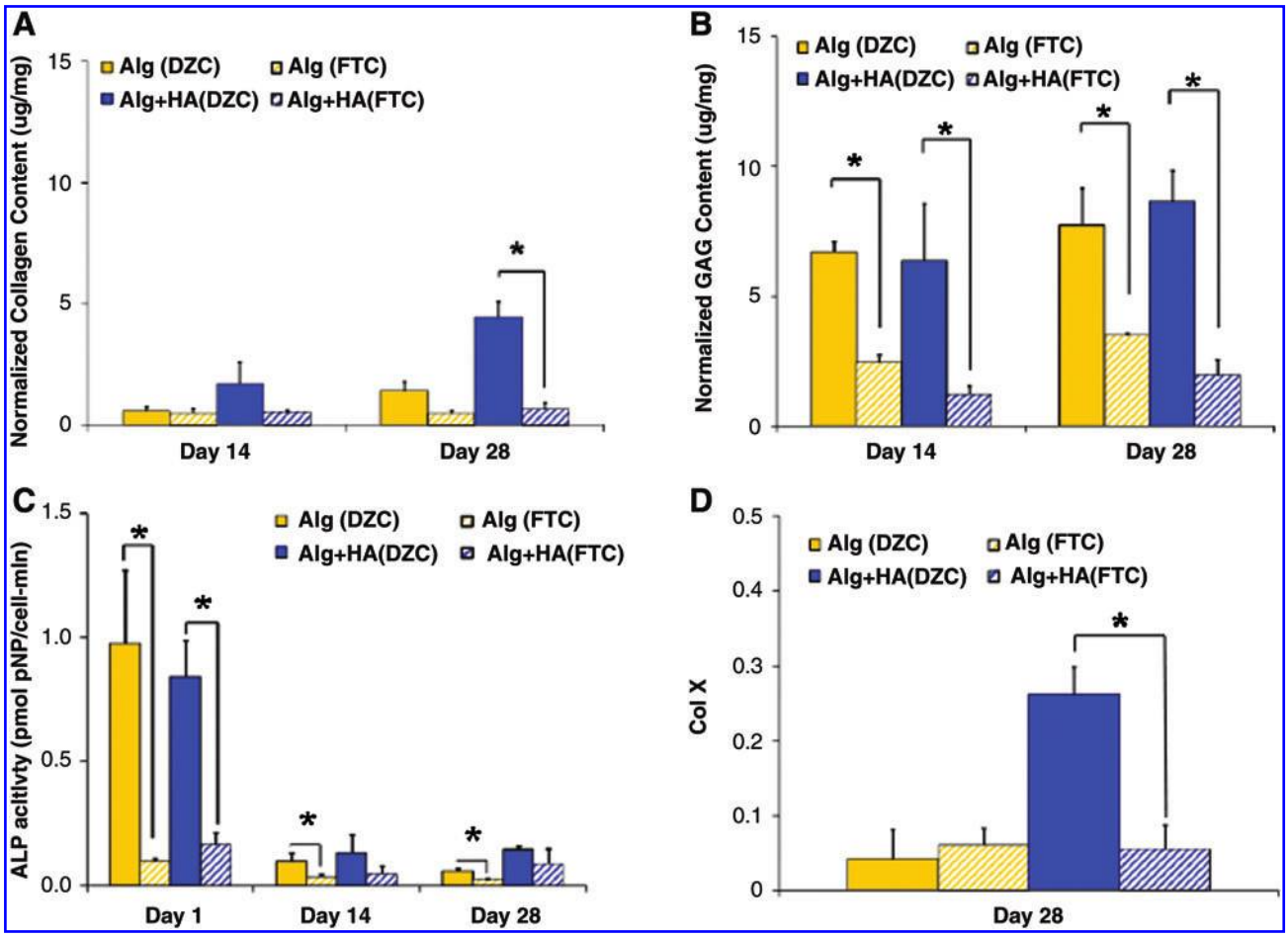

FIG. 8. Effect of chondrocyte population. **(A)** By day 28, higher collagen content was measured for the alginate + HA scaffolds seeded with DZC instead of full-thickness chondrocytes (FTC) (*$p < 0.05$, $n = 5$). **(B)** Higher proteoglycan deposition was detected in the DZC-seeded alginate and alginate + HA groups as compared with those seeded with FTC (*$p < 0.05$, $n = 5$). **(C)** Higher ALP activity was measured for DZC as compared with FTC at day 1 (*$p < 0.05$, $n = 5$). **(D)** By day 28, higher type X collagen expression was measured for the alginate + HA scaffolds seeded with DZC instead of FTC (*$p < 0.05$, $n = 5$). Color images available online at www.liebertonline.com/tea

increase in cell size and the upregulation of both type X collagen and MMP-13 over time. This maybe analogous to endochondral ossification, during which proliferating chondrocytes mature into hypertrophic chondrocytes that express type X collagen and MMP-13, exhibit ALP activity, and eventually mineralize.[49–53] However, unlike bone, there was no evidence of type I collagen deposition and the scaffold remains rich in type II collagen, thereby more closely resembling cartilage. Interestingly, the presence of HA in the alginate hydrogel promoted chondrocyte hypertrophy without an accompanying significant increase in mineralization potential. It is possible that the preincorporated ceramic phase of the composite scaffold is biomimetic, and its availability diminishes the need for further cell-mediated mineralization.

As full-thickness chondrocytes have been widely used for cartilage tissue engineering, another objective of this study was to determine the optimal chondrocyte population for osteochondral interface regeneration. To this end, the response of full-thickness chondrocytes was compared with that of DZC in alginate and alginate + HA scaffolds. It was found that DZC produced more collagen and proteoglycan, and exhibited higher ALP activity than full-thickness chondrocytes. The higher mineralization potential and proteoglycan synthesis observed here for DZC in the alginate controls are in agreement with published studies.[33,54] Interestingly, mineralization potential and hypertrophic marker expression were only upregulated when DZC were cultured in alginate + HA scaffolds. Further, our previous studies of surface zone and middle zone chondrocyte seeded in hydrogel scaffolds measured basal ALP activity over time, regardless of HA presence.[55] These results suggest that DZC-like cells seeded in the alginate + HA scaffold represents an optimal combination for osteochondral interface tissue engineering. It is noted that when comparing zonal populations of cells, it is also critical to recognize the presence of progenitor cells that reside in cartilage,[56] especially as the enzymatic digest used in this study will yield a mixed population of cells. However, given the serum-free conditions, lack of growth factor stimulation, and relatively low cell seeding density in this study, it is not anticipated that progenitor cells will contribute significantly to the observed cell response.

Clinically, it is envisioned that the interface scaffold described in this study can be utilized in combination with other cartilage tissue engineering grafts. For example, the hydrogel–ceramic scaffold can be placed above subchondral bone, with a cartilage scaffold or graft layered above. It is anticipated that the ceramic phase will promote osteointegration, while the hydrogel phase of the composite would facilitate integration with a hydrogel-based cartilage graft. Additional future studies will focus on optimizing the composite hydrogel scaffold system in terms of ceramic dose and distribution, cell type (e.g., adult human chondrocytes), cell density, and culturing time, with the long-term goal of utilizing the optimized scaffold for osteochondral interface tissue engineering.

Conclusions

In summary, it is observed that the alginate + HA composite scaffold promotes DZC-mediated formation of a calcified cartilage-like matrix, with higher mechanical properties than ceramic-free alginate scaffolds. These findings collectively demonstrate that the hydrogel–ceramic composite is promising for osteochondral interface tissue engineering and integrative cartilage repair.

Acknowledgments

The type X collagen antibody was obtained from the Developmental Studies Hybridoma Bank developed under the auspices of the NICHD and maintained by The University of Iowa, Department of Biology, Iowa City, IA 52242. The authors would like to thank Stephen Doty, Ph.D., and Anthony Labissiere (Hospital for Special Surgery, NY) for their assistance with ESEM. This study was funded by the Wallace H. Coulter Foundation (H.H.L.), NIH-NIAMS 5R01AR055280 (H.H.L.), and National Science Foundation Graduate Research Fellowship (N.T.K.).

Disclosure Statement

No competing financial interests exist.

References

1. Sacks, J.J., Luo, Y.H., and Helmick C.G. Prevalence of specific types of arthritis and other rheumatic conditions in the ambulatory health care system in the United States, 2001–2005. Arthritis Care Res (Hoboken) **62,** 460, 2010.
2. Schiller, J.S., Adams, P.F., and Nelson, Z.C. Summary health statistics for the U.S. population: National Health Interview Survey, 2003. Vital Health Stat **10,** 1, 2005.
3. Mow, V.C., Gu, W.Y., and Chen, F.H. Structure and function of articular cartilage and meniscus. In: Mow, V.C., and Huiskes, R., eds. Basic Orthopaedic Biomechanics and Mechano-Biology. Philadelphia: Lippincott Williams and Wilkins, 2004.
4. Steadman, J.R., Briggs, K.K., Rodrigo, J.J., *et al.* Outcomes of microfracture for traumatic chondral defects of the knee: average 11-year follow-up. Arthroscopy **19,** 477, 2003.
5. Bedi, A., Feeley, B.T., and Williams, R.J., III. Management of articular cartilage defects of the knee. J Bone Joint Surg Am **92,** 994, 2010.
6. Hunziker, E.B. Articular cartilage repair: basic science and clinical progress. A review of the current status and prospects. Osteoarthritis Cartilage **10,** 432, 2002.
7. Havelka, S., Horn, V., Spohrova, D., and Valouch, P. The calcified-noncalcified cartilage interface: the tidemark. Acta Biol Hung **35,** 271, 1984.
8. Norrdin, R.W., Kawcak, C.E., Capwell, B.A., and McIlwraith, C.W. Calcified cartilage morphometry and its relation to subchondral bone remodeling in equine arthrosis. Bone **24,** 109, 1999.
9. Mente, P.L., and Lewis, J.L. Elastic modulus of calcified cartilage is an order of magnitude less than that of subchondral bone. J Orthop Res **12,** 637, 1994.
10. Redler, I., Mow, V.C., Zimny, M.L., and Mansell, J. The ultrastructure and biomechanical significance of the tidemark of articular cartilage. Clin Orthop Relat Res **112,** 357, 1975.
11. Bullough, P.G., and Jagannath, A. The morphology of the calcification front in articular cartilage. Its significance in joint function. J Bone Joint Surg Br **65,** 72, 1983.
12. Oegema, T.R., Jr., Carpenter, R.J., Hofmeister, F., and Thompson, R.C., Jr. The interaction of the zone of calcified cartilage and subchondral bone in osteoarthritis. Microsc Res Tech **37,** 324, 1997.
13. Hunziker, E.B., Driesang, I.M., and Saager, C. Structural barrier principle for growth factor-based articular cartilage repair. Clin Orthop Relat Res Supplement, S182, 2001.
14. Kandel, R.A., Hurtig, M., and Grynpas, M. Characterization of the mineral in calcified articular cartilagenous tissue formed *in vitro*. Tissue Eng **5,** 25, 1999.
15. Allan, K.S., Pilliar, R.M., Wang, J., *et al.* Formation of biphasic constructs containing cartilage with a calcified zone interface. Tissue Eng **13,** 167, 2007.
16. Smidsrod, O., and Skjak-Braek, G. Alginate as immobilization matrix for cells. Trends Biotechnol **8,** 71, 1990.
17. Wan, L.Q., Jiang, J., Arnold, D.E., *et al.* Calcium concentration effects on the mechanical and biochemical properties of chondrocyte-alginate constructs. Cell Mol Bioeng **1,** 93, 2008.
18. Guo, J.F., Jourdian, G.W., and MacCallum, D.K. Culture and growth characteristics of chondrocytes encapsulated in alginate beads. Connect Tissue Res **19,** 277, 1989.
19. Hauselmann, H.J., Aydelotte, M.B., Schumacher, B.L., *et al.* Synthesis and turnover of proteoglycans by human and bovine adult articular chondrocytes cultured in alginate beads. Matrix **12,** 116, 1992.
20. Paige, K.T., and Vacanti, C.A. Engineering new tissue: formation of neo-cartilage. Tissue Eng **1,** 97, 1995.
21. Masuda, K., Sah, R.L., Hejna, M.J., and Thonar, E.J. A novel two-step method for the formation of tissue-engineered cartilage by mature bovine chondrocytes: the alginate-recovered-chondrocyte (ARC) method. J Orthop Res **21,** 139, 2003.
22. Loty, S., Sautier, J.M., Loty, C., *et al.* Cartilage formation by fetal rat chondrocytes cultured in alginate beads: a proposed model for investigating tissue-biomaterial interactions. J Biomed Mater Res **42,** 213, 1998.
23. Lu, H.H., Vo, J.M., Chin, H.S., *et al.* Controlled delivery of platelet-rich plasma-derived growth factors for bone formation. J Biomed Mater Res A **86,** 1128, 2008.
24. Boskey, A.L. Mineral-matrix interactions in bone and cartilage. Clin Orthop Relat Res **(281),** 244, 1992.
25. Boskey, A.L., and Bullough, P.G. Cartilage calcification: normal and aberrant. Scan Electron Microsc **(Pt 2),** 943, 1984.
26. Huang, Z., Tian, J., Yu, B., *et al.* A bone-like nano-hydroxyapatite/collagen loaded injectable scaffold. Biomed Mater **4,** 055005, 2009.
27. Song, J., Xu, J., Filion, T., *et al.* Elastomeric high-mineral content hydrogel-hydroxyapatite composites for orthopedic applications. J Biomed Mater Res A **89,** 1098, 2009.

28. Patel, M., Patel, K.J., Caccamese, J.F., *et al.* Characterization of cyclic acetal hydroxyapatite nanocomposites for craniofacial tissue engineering. J Biomed Mater Res A **94,** 408, 2010.
29. Wang, X., Grogan, S.P., Rieser, F., *et al.* Tissue engineering of biphasic cartilage constructs using various biodegradable scaffolds: an *in vitro* study. Biomaterials **25,** 3681, 2004.
30. Tanaka, T., Komaki, H., Chazono, M., and Fujii, K. Use of a biphasic graft constructed with chondrocytes overlying a beta-tricalcium phosphate block in the treatment of rabbit osteochondral defects. Tissue Eng **11,** 331, 2005.
31. Guo, X., Wang, C., Duan, C., *et al.* Repair of osteochondral defects with autologous chondrocytes seeded onto bioceramic scaffold in sheep. Tissue Eng **10,** 1830, 2004.
32. Buckwalter, J.A., and Mankin, H.J. Articular cartilage: tissue design and chondrocyte-matrix interactions. Instr Course Lect **47,** 477, 1998.
33. Jiang, J., Leong, N.L., Mung, J.C., *et al.* Interaction between zonal populations of articular chondrocytes suppresses chondrocyte mineralization and this process is mediated by PTHrP. Osteoarthritis Cartilage **16,** 70, 2008.
34. Jiang, J., Nicoll, S.B., and Lu, H.H. Co-culture of osteoblasts and chondrocytes modulates cellular differentiation *in vitro*. Biochem Biophys Res Commun **338,** 762, 2005.
35. Ramshaw, J.A., Bateman, J.F., and Cole, W.G. Precipitation of collagens by polyethylene glycols. Anal Biochem **141,** 361, 1984.
36. Enobakhare, B.O., Bader, D.L., and Lee, D.A. Quantification of sulfated glycosaminoglycans in chondrocyte/alginate cultures, by use of 1,9-dimethylmethylene blue. Anal Biochem **243,** 189, 1996.
37. Farndale, R.W., Sayers, C.A., and Barrett, A.J. A direct spectrophotometric microassay for sulfated glycosaminoglycans in cartilage cultures. Connect Tissue Res **9,** 247, 1982.
38. Seibel, M.J., Macaulay, W., Jelsma, R., *et al.* Antigenic properties of keratan sulfate: influence of antigen structure, monoclonal antibodies, and antibody valency. Arch Biochem Biophys **296,** 410, 1992.
39. Wan, L.Q., Jiang, J., Miller, D.E., *et al.* Matrix deposition modulates the viscoelastic shear properties of hydrogel-based cartilage grafts. Tissue Eng Part A **17,** 1111, 2011.
40. Armstrong, C.G., Bahrani, A.S., and Gardner, D.L. *In vitro* measurement of articular cartilage deformations in the intact human hip joint under load. J Bone Joint Surg Am **61,** 744, 1979.
41. Lu, H.H., Kofron, M.D., El Amin, S.F., *et al. In vitro* bone formation using muscle-derived cells: a new paradigm for bone tissue engineering using polymer-bone morphogenetic protein matrices. Biochem Biophys Res Commun **305,** 882, 2003.
42. Wang, I.E., Shan, J., Choi, R., *et al.* Role of osteoblast-fibroblast interactions in the formation of the ligament-to-bone interface. J Orthop Res **25,** 1609, 2007.
43. Lu, H.H., Tang, A., Oh, S.C., *et al.* Compositional effects on the formation of a calcium phosphate layer and the response of osteoblast-like cells on polymer-bioactive glass composites. Biomaterials **26,** 6323, 2005.
44. Zhu, W., Mow, V.C., Koob, T.J., and Eyre, D.R. Viscoelastic shear properties of articular cartilage and the effects of glycosidase treatments. J Orthop Res **11,** 771, 1993.
45. Zhu, W., Iatridis, J.C., Hlibczuk, V., *et al.* Determination of collagen-proteoglycan interactions *in vitro*. J Biomech **29,** 773, 1996.
46. Buckwalter, J.A. Proteoglycan structure in calcifying cartilage. Clin Orthop Relat Res **(172),** 207, 1983.
47. Boontheekul, T., Kong, H.J., and Mooney, D.J. Controlling alginate gel degradation utilizing partial oxidation and bimodal molecular weight distribution. Biomaterials **26,** 2455, 2005.
48. Ferguson, V.L., Bushby, A.J., and Boyde, A. Nanomechanical properties and mineral concentration in articular calcified cartilage and subchondral bone. J Anat **203,** 191, 2003.
49. Tacchetti, C., Quarto, R., Campanile, G., and Cancedda, R. Calcification of *in vitro* developed hypertrophic cartilage. Dev Biol **132,** 442, 1989.
50. Bellows, C.G., Aubin, J.E., and Heersche, J.N. Initiation and progression of mineralization of bone nodules formed *in vitro*: the role of alkaline phosphatase and organic phosphate. Bone Miner **14,** 27, 1991.
51. Schmid, T.M., Bonen, D.K., Luchene, L., and Linsenmayer, T.F. Late events in chondrocyte differentiation: hypertrophy, type X collagen synthesis and matrix calcification. In Vivo **5,** 533, 1991.
52. Linsenmayer, T.F., Long, F., Nurminskaya, M., *et al.* Type X collagen and other up-regulated components of the avian hypertrophic cartilage program. Prog Nucleic Acid Res Mol Biol **60,** 79, 1998.
53. D'Angelo, M., Yan, Z., Nooreyazdan, M., *et al.* MMP-13 is induced during chondrocyte hypertrophy. J Cell Biochem **77,** 678, 2000.
54. Waldman, S.D., Grynpas, M.D., Pilliar, R.M., and Kandel, R.A. The use of specific chondrocyte populations to modulate the properties of tissue-engineered cartilage. J Orthop Res **21,** 132, 2003.
55. Khanarian, N.T., Jiang, J., McArdle, S.A., Hung, C.T., and Lu, H.H. Zonal chondrocyte interactions regulate chondrocyte calcification via PTHrP**.** Transactions of the 56th Annual Meeting of the Orthopaedic Research Society, New Orleans, Louisiana, 2010.
56. Grogan, S.P., Miyaki, S., Asahara, H., *et al.* Mesenchymal progenitor cell markers in human articular cartilage: normal distribution and changes in osteoarthritis. Arthritis Res Ther **11,** R85, 2009.

Address correspondence to:
Helen H. Lu, Ph.D.
Biomaterials and Interface Tissue Engineering Laboratory
Department of Biomedical Engineering
Columbia University
1210 Amsterdam Ave.
351 Engineering Terrace, MC 8904
New York, NY 10027

E-mail: hhlu@columbia.edu

Received: May 16, 2011
Accepted: September 15, 2011
Online Publication Date: November 4, 2011

This article has been cited by:

1. Eamon J. Sheehy, Tatiana Vinardell, Conor T. Buckley, Daniel J. Kelly. 2012. Engineering osteochondral constructs through spatial regulation of endochondral ossification. *Acta Biomaterialia* . [CrossRef]
2. M. D###Este, D. Eglin. 2012. Hydrogels in calcium phosphate moldable and injectable bone substitutes: Sticky excipients or advanced 3-D carriers?. *Acta Biomaterialia* . [CrossRef]
3. Nathan J. Castro, S. Adam Hacking, Lijie Grace Zhang. 2012. Recent Progress in Interfacial Tissue Engineering Approaches for Osteochondral Defects. *Annals of Biomedical Engineering* **40**:8, 1628-1640. [CrossRef]
4. Nora T. Khanarian, Nora M. Haney, Rachel A. Burga, Helen H. Lu. 2012. A functional agarose-hydroxyapatite scaffold for osteochondral interface regeneration. *Biomaterials* **33**:21, 5247-5258. [CrossRef]
5. Orapin V. Horst, Miquella G. Chavez, Andrew H. Jheon, Tejal Desai, Ophir D. Klein. 2012. Stem Cell and Biomaterials Research in Dental Tissue Engineering and Regeneration. *Dental Clinics of North America* **56**:3, 495-520. [CrossRef]